Title

Efficacy of a Lung-Tuned Monopole Antenna for Microwave Ablation: Analytical Solution and Validation in a Ventilator-Controlled Ex Vivo Porcine Lung Model

Journal

IEEE Journal of Electromagnetics RF and Microwaves in Medicine and Biology, 5(4)

ISSN

2469-7249

Authors

Chiang, Jason
Song, Lingnan
Abtin, Fereidoun
et al.

Publication Date

2021-12-01

DOI

10.1109/jerm.2021.3066103

Peer reviewed

Published in final edited form as:

IEEE J Electromagn RF Microw Med Biol. 2021 December ; 5(4): 295–304. doi:10.1109/jerm.2021.3066103.

Efficacy of Lung-Tuned Monopole Antenna for Microwave Ablation: Analytical Solution and Validation in a Ventilator-Controlled *ex Vivo* Porcine Lung Model

Jason Chiang [Member, IEEE],
Department of Radiology, Ronald Reagan UCLA Medical Center

Lingnan Song [Member, IEEE],
Department of Electrical and Computer Engineering, University of California, Los Angeles, Los Angeles, CA 90095 USA

Fereidoun Abtin,
Department of Radiology, Ronald Reagan UCLA Medical Center

Yahya Rahmat-Samii [Life Fellow, IEEE]
Department of Electrical and Computer Engineering, University of California, Los Angeles, Los Angeles, CA 90095 USA

Abstract

The goal of this study was to optimize a lung-tuned monopole antenna to deliver microwave energy at 2.45 GHz into a novel ventilator-controlled *ex vivo* lung model. An analytic and parametric approach was utilized to create an optimized monopole antenna that was impedance-matched to aerated lung tissue. This lung-tuned antenna was then fabricated using a copper 0.085" semi-rigid copper coaxial cable. For validation, the lung-tuned antenna was inserted centrally into lobes of a *ex vivo* porcine lung that was fully inflated to physiologically appropriate volumes. Microwave ablations were then created at 50 and 100 W for 1 minute and 5 minutes. Reflected power, cross sectional ablation sizes and spherical shape of the lung-tuned antenna were compared against a liver-tuned antenna in the ventilator-controlled *ex vivo* lung tissue. The study showed that the lung-tuned antennas delivered energy significantly more efficiently, with less reflected power, compared to the conventionally-used liver-tuned antennas at 50 W at 1 minute (11.8±3.0 vs 16.3±3.1 W; p value=0.03) and 5 minutes (16.2±2.8 vs 19.4±2.9 W; p value=0.04), although this was only true using 100 W at the 1 minute time point (29.0±3.5 vs 38.0±5.3 W; p value=0.02). While overall ablation zone sizes were comparable between the two types of antenna, the lung-tuned antenna did create a significantly more spherical ablation zone compared to the liver-tuned antenna at the 1 minute, 50 W setting (aspect ratio: 0.43±0.07 vs 0.38±0.04; p value=0.04). In both antenna groups, there was a significant rise in the ablation zone aspect ratio between 1 and 5 minutes, indicating that higher power and time settings can increase the spherical shape of ablation zones when using tuned antennas. Adapting this combined analytic and parametric approach to

CJChiang@mednet.ucla.edu .

antenna design can be implemented in adaptive tissue-tuning for real-time microwave ablation optimization in lung tissue.

Keywords

Thermal ablation; monopole antenna; computational modeling; microwave; antenna design; *ex vivo* tissue

I. Introduction

Lung cancer remains the leading cause of cancer deaths among men and women, comprising of nearly 25% of all cancer deaths [1]. While surgical lobectomy remains the standard of care, only a fraction of the patients are considered eligible due to associated comorbidities such as poor pulmonary reserve, concommitent pulmonary fibrosis, or advanced frailty [2]. Percutaneous image-guided thermal ablations have become an attractive option due to their association with fewer complications, quicker recovery and minimal blood loss [3]. During thermal ablation procedures, energy is transmitted through an antenna or applicator under image guidance toward target tumor tissue. The ablation process continues until the tumor tissue is heated to cytotoxic temperatures with sufficient margins, all while minimizing damage to normal surrounding tissue [4]. For treating lung malignancies, thermal ablations are also associated minimal effect on pulmonary function, a side effect that can be seen in both radiation therapy or surgical resection [5].

Major considerations when choosing ablation modalities include the size and anatomic location of the target tumors. Larger tumors are associated with more advanced cancer stages and higher rates of recurrence. For that reason, using microwave ablation has gained traction over radiofrequency ablation and cryoablation because of its ability to be tuned to the target tissue, delivering higher levels of power into the tissue and creating larger, more homogeneous ablation zones [6], [7]. In addition, when compared to radiofrequency ablation, microwave ablation has been associated with less post-procedural pain [8]. Despite these advantages, the outcome data from microwave ablation remains heterogeneous due to variations in target patient population and follow up periods. Current single-institution studies using microwave ablation have survival rates ranging from 47-83% at 1 year, 24-73% at 2 years and 14-62% at 3 years [8]–[10].

The concept of tuning a microwave antenna toward a target tissue has been well established in present literature [4], [11]–[16]. Reflected power is often a heavily weighted variable in antenna optimization strategies because it can be related to how well matched an antenna or transmission line is to the target organ [15]. Low reflected power can be indicative of optimal impedance matching and translates into efficient power deposition into the tissue. Conversely, high reflected power can signify an impedance mismatch between the target tissue and antenna, leading to decreased power delivered into the tissue. A mismatch between the antenna and the tissue can also cause power to be reflected back into the generator and cause the formation of a standing wave into the feeding line, leading to excess heating loss along the shaft of the antenna. The other important metric in antenna optimization strategy is the shape of the ablation zone within the tissue. More spherical

ablation zones are desirable as it can encompass a round tumor with appropriate margins and minimize the risk for backward heating. Heat that spreads backward along the shaft of the antenna can damage the superficial surfaces of the organ, often times leading to post-procedural pain. In the lungs, inadvertent backward heating can lead to more severe complications such as pneumothorax or bronchopleural fistulas.

Validation studies for organ-tuned antennas have largely been performed on *in vivo* and *ex vivo* liver tissue. Within lung tissue, however, optimization and validation of lung-tuned antennas currently remains in its nascency. Part of the reason is that lung tissue composition varies by gas exchange during respiration and anatomic location, with the central regions being more heterogeneous compared to peripheries [17]. The validation component of lung-tuned antennas is also challenging in an *ex vivo* model where gas content needs to be maintained. As a result, current literature on the performance and clinical outcomes of lung ablations is limited and confounded by heterogeneous data.

In this study, we revisited the usage of an existing analytical solution and tailored it to optimize a monopole antenna to transmit energy efficiently into the dielectric load of an air-expanded lung while maintaining a spherical ablation zone. This lung-tuned antenna was then used to create microwave ablation zones in a ventilator-controlled *ex vivo* porcine lung model. The advantages of lung-tuning were then quantified by comparing its performance against a liver-tuned antenna control. The contributions of the work are embodied in three major step-wise components: (a) utilizing an analytic solution to optimize a monopole antenna design that efficiently delivers microwave energy into lung tissue, (b) combining the analytic solution with a parametric approach to simultaneously create a spherical ablation zone within the lung while preserving heating efficiency, and lastly (c) experimentally validating these optimized antenna designs utilizing a novel ventilator-controlled *ex vivo* lung model. Starting with an analytical solution in microwave antenna tuning minimizes the computational steps required to optimize an antenna design. The findings of this study lay the foundation for adaptive tissue-tuning for real-time microwave antenna ablation optimization.

II. Methods

A. Numerical Simulation

1) Analytical Modeling: Modern microwave ablation antennas utilize semi-rigid copper coaxial cables to act as the transmission line between the power generator and the target tissue. The impedance load of the microwave antenna is modulated by changing the geometry at the end of the coaxial cable. The monopole antenna is one of the most widely used class of antennas and its general geometry can be constructed by stripping off a section of outer conductor at the end of coaxial cable. The dimensions of the 0.085” copper coaxial cable are listed in Table I. The length of the underlying exposed dielectric is specified by length of $L_{ant} = \lambda_{eff}/4$, where λ_{eff} represents the effective wavelength for the design of the coaxial antenna. Fig. 1 illustrates the generalized structure of a coaxial monopole antenna.

The optimal exposed dielectric length was analytically calculated by evaluating the insulating antenna as an inner conductor wrapped within multiple dielectric layers and

immersed in a lossy dielectric medium [18]. This methodology treats the insulating antenna as multiple sections of a lossy transmission line with generalized propagation constants to account for both ohmic losses as well as radiative losses from the antenna to the ambient medium. The multi-layered insulated antenna is then able to be represented by a multi-sectioned transmission line, with each section terminated with a load impedance equivalent to the input impedance of the preceding section [19]. In the case of the monopole design, the insulating monopole antenna consists of a central conductive cylinder with radius a and length h (representing the inner conductor of coaxial cable), wrapped by cylindrical dielectric region with radius b and dielectric constant ϵ_2 (representing the Teflon filled in coaxial cable), immersed in infinite homogeneous medium with dielectric constant ϵ_3 and conductivity σ_3. The three regions corresponding to different dielectric properties are identified in Fig. 1. In this case, the electrical properties of an inflated lungs were utilized as a surrogate variable to account for the presence of air that is present within the lungs.

The wavenumber in the insulating and lossy dielectric regions is therefore:

$$k_2 = \omega\sqrt{\mu_0\epsilon_2}, \quad k_3 = \omega\sqrt{\mu_0(\epsilon_3 - j\sigma_3/\omega)} \tag{1}$$

where μ_0 is the free space permeability assumed to apply in all regions. Throughout the paper an $e^{j\omega t}$ time convention is applied. This approach also requires that the wavenumber in ambient medium is greater than that of the insulating dielectric, and that the cross section of the antenna is electrically small:

$$|k_3/k_2|^2 \gg 1, \quad (k_2 b)^2 \ll 1 \tag{2}$$

Assuming the antenna is excited with voltage source V_0^e, the current carried by the antenna central conductor is thus given as [18]:

$$I(z) = I(0)\frac{\sin k_{\text{eff}}(h - |z|)}{\sin k_{\text{eff}} h} = j\frac{V_0^e}{2Z_c}\frac{\sin k_{\text{eff}}(h - |z|)}{\cos k_{\text{eff}} h} \tag{3}$$

where $I(0)$ represents the current at $z = 0$. The characteristic impedance Z_c and the effective propagation constant k_{eff} are given by [18]:

$$Z_c = \frac{\omega\mu_0 k_{\text{eff}}}{2\pi k_2^2}\left[\ln\frac{b}{a} + \frac{k_2^2}{k_3^2}\frac{H_0^{(1)}(k_3 b)}{k_3 b H_1^{(1)}(k_3 b)}\right] \tag{4}$$

$$k_{\text{eff}} = k_2\left[\frac{\ln\left(\frac{b}{a}\right)k_3 b H_1^{(1)}(k_3 b) + H_0^{(1)}(k_3 b)}{\ln\left(\frac{b}{a}\right)k_3 b H_1^{(1)}(k_3 b) + \frac{k_2^2}{k_3^2}H_0^{(1)}(k_3 b)}\right]^{1/2} \tag{5}$$

$$k_{\text{eff}} = \beta_{\text{eff}} + j\alpha_{\text{eff}} \tag{6}$$

where $H^{(1)}$ represents Hankel function of the first kind. To corroborate its validity, it can be readily verified that in a case where k_3 approaches to k_2, the effective propagation constant k_{eff} also approaches to k_2, reducing the case to a monopole immersed in dielectric material. The real part of the effective propagation constant β_{eff} can then be directly linked to the effective wavelength $\lambda_{\text{eff}} = 2\pi/\beta_{\text{eff}}$, from which the optimal exposed dielectric length of monopole antenna is determined.

2) Antenna Optimization: The major requirements for optimizing microwave ablation antennas included: (a) small diameter for ease of percutaneous insertion; (b) good impedance matching for efficient power transmission; (c) localized spherical ablation pattern for more precise ablation treatment. A computational parametric approach was utilized to find the optimal ablation design, weighing not only the reflection coefficient but also the shape of the ablation zone. The specific absorption rate (SAR) was calculated for various lengths of the exposed monopole dielectric in the vicinity of the optimal length described above. These lengths were altered in 0.5 mm intervals as that was our fabrication tolerance in the laboratory. Simulations were performed in a two dimensional domain assuming a rotational symmetry on the longitudinal axis of the antenna. Analysis was performed using finite-element approach to solve Maxwell's equations in the transverse magnetic (TM) propagation mode (COMSOL Multiphysics 5.5; Burlington, MA)

$$\nabla^2\mathbf{E} = -\omega^2\mu_0(\epsilon_0\epsilon_r(f) - j\frac{\sigma(f)}{\omega})\mathbf{E}, \tag{7}$$

where $\mathbf{E}$ is the electric field vector (V/m), ω is the angular frequency (rad/sec), ϵ_r is the relative permittivity and σ is the effective conductivity (S/m). Lung and liver properties from Table I were utilized to visualize the SAR map. To create the most spherical ablation zone, we calculated an aspect ratio (AR) from the SAR map, which we defined as twice the maximum radial dimension (diameter) divided by the longitudinal dimension (length) of the SAR = 300 W/kg isocontour in the SAR maps.

An optimization function Ψ was utilized to find the antenna that balanced antenna impedance matching at 2.45 GHz in terms of S_{11} (in dB scale) with the most spherical ablation zone, characterized by the highest AR [20]. Ψ was defined as:

$$\Psi(S_{11}, AR) = \frac{1}{1 + e^{A_1(S_{11} + B_1)}} + \frac{1}{1 + e^{A_2(AR + B_2)}}, \tag{8}$$

where A_1 and A_2 represented slopes of the sigmoidal curves at inflection points B_1 and B_2. In general, reflection coefficients greater than −20 dB or heating aspect ratios less than 0.7 were considered too inefficient or too elongated of an ablation zone, respectively. With these constraints, the coefficient values selected for the above equation were $A_1 = 0.7$, $A_2 = -20$, $B_1 = -15$ and $B_2 = 0.7$. This equation can be adapted for various organs, based on expected S11 and aspect ratio. The optimization function in this case was able to provide discriminatory value in filtering out antennas that were too elongated in shape or had too high of a reflection coefficient.A propensity score was calculated for each permutation in the parametric analysis, with the highest score indicating the most optimal design that balanced reflected power against most spherical ablation zone design.

B. Experimental Setup

Lung-tuned and liver-tuned monopole antennas were constructed from polytetrafluorethylene (PTFE) filled, semi-rigid coaxial cable (UT-085C; Micro-Coax LLC, Pottstown, PA) with exposed dielectric lengths calculated from the analytical solution. An industrial high-powered solid state 2.45 GHz microwave generator (Sairem, Neyron, France) was used to create the ablation zones.

Microwave ablation experiments were performed on freshly excised *ex vivo* porcine lung tissues with attached airways. The lungs were removed en-bloc and allowed to reach room temperature (25° C) over a period of 1-2 hours. The lung tissue was mechanically ventilated to maintained a 600 mL volume controlled airspace to mimic a fully expanded lung. The lung tuned 15.5 mm antennas were inserted 5 cm into the central portions of the upper, middle and lower fields of the right lung. Microwave ablations were created at 50 W and 100 W for 1 and 5 minute with reflected power being recorded in 10-second intervals from the microwave generator display (2). Corresponding matched ablations were then created in the left lung with the liver-tuned 13.0 mm monopole antennas as controls using the same power and time settings. Sample images of the two antennas and ventilated lung are shown in Fig. 2. Ablation zones (n=7 for each power/time combination) were created in the *ex vivo* lung tissue using the lung-tuned antenna and liver-tuned antenna.

After the ablations were completed, ablation zones were sectioned across their insertion path, revealing a cross section of the ablation zone. The congestive component of the ablation zone was measured and served as the outer border of the ablation zone. Ablation length and width were recorded and compared between antennas. Student t-test was performed to evaluate differences in each ablation zone metric. P-values less than 0.05 were considered significant.

III. Results

A. Analytical Modeling

1) Analytical Modeling: The effective quarter wavelength was computed with $\lambda_{\text{eff}}/4 = \pi/2\beta_{\text{eff}}$ and plotted in Fig. 3 for 0.085” cable with varying tissue dielectric constant and conductivity. In an air-filled lung environment, an exposed dielectric length of 15.5 mm was found to provide the optimal impedance match. In a liver environment, an exposed dielectric length of 13.0 mm was identified, consistent with presently known literature on liver-tuned antennas [12], [15]. Note in Fig. 3 that the effective quarter wavelength for the lung was not sensitive to the variation of tissue dielectric property, which varied only within the range of ±1 mm for ϵ_r from 10 to 90 and σ_r from 4 to 0.5 S/m.

2) Antenna Optimization: The optimal design for the lung and liver was based on the optimization function in equation (8) and the global maximum was found at the exposed dielectric length of 15.5 mm and 13 mm, respectively. From the parametric study, it was seen that the reflection coefficient was very sensitive to the exposed dielectric length, with the global minimum seen at the 15.5 mm length when using a lung-tissue medium, as seen

in Fig. 4. The parametric study also confirmed the analytic solution to this study in targeting the optimal length for minimizing the reflection coefficient.

On the other hand, the aspect ratio of the monopole antenna demonstrated a monotonic increase in value with increasing exposed dielectric length. The aspect ratio only increased minimally with each unit increase in length, while the reflection coefficient increased by up to 10 dB for each millimeter increase in length. The cost function also demonstrated similar drop off in value after 15.5 mm, confirming the minimal improvement in performance even when accounting for aspect ratio.

In order to expand on the parametric study of the monopole antenna targeting the lungs with air, the relationship between air content percentage was first related to the constitutive parameters of the lung model. These parameters included the relative dielectric constant and the conductivity. Air content of 0% represented the fully deflated state and air content of 100% represented the fully inflated state of the lung. Intermediate states with the lung model partially inflated were evaluated using logistic regression modeling. The resulting curves of the relative dielectric constant and conductivity were calculated for air content varying from 0% to 100%. Full-wave simulations for 13.0 mm and 15.5 mm monopole antennas were carried out for each of the air content states, and results were compared in Fig. 5. It was clearly observed that 15.5 mm monopole results in improved S parameter for high air content (80% and 100% air filling), while 13 mm performed better in a deflated lung compared to an inflated lung.

B. Experimental Results

Within the *ex vivo* ventilator-inflated lung tissue, both the 13.0 mm liver-tuned and 15.5 mm lung-tuned antenna exhibited a monotonic increase in reflected power over time in both the 50 W and 100 W groups. At 50 W, the lung-tuned antenna trended toward less reflection power at the 1 minute mark (mean ± standard deviation, 12.7±3.1 vs 16.6±6.5 W, p=0.33) and the 5 minute mark (16.2±2.8 vs 19.4±2.9 W, p=0.04)(Fig. 6). At 100 W, the lung-tuned antenna had a significantly less reflected power at the 1 minute mark (29.0±3.5 vs 38.0±5.3 W, p=0.02) but this trend did not continue to 5 minutes, where the reflected power was not significantly different (40.8±7.5 vs 44.8±5.1 W, p=0.35).

In the 50 W cohort at 1 minute, the lung-tuned antennas, compared to the liver-tuned antennas, created a slightly larger ablation zone width (1.4±0.2 vs 1.3±0.2 cm, p=0.40) and a shorter ablation length (3.4±0.5 vs 3.6±0.9 cm, p=0.53), although neither differences were found to be statistically significant. However, this resulted in the lung-tuned antenna having a significantly larger ablation aspect ratio compared to the liver-tuned antenna (0.43±0.07 vs 0.38±0.04, p=0.04). In the 50 W, 5 minute ablation group, the lung-tuned antenna created similar sized ablation zone widths (2.8±0.2 vs 2.9±0.3 cm, p=0.77) and ablation zone lengths (5.1±0.6 vs 5.4±0.6 cm, p=0.47), resulting in aspect ratios that were not significantly different from each other (0.56±0.06 vs 0.54±0.09, p=0.74). Within the samples that underwent 1 minute ablations at 100 W, the lung-tuned antennas created ablation zones with widths and lengths that were not significantly different from the liver tuned antennas (2.8±0.2 vs 2.8±0.4 cm, p=0.77 and 5.1±0.6 vs 5.3±0.6 cm, p=0.65, respectively). In the group that underwent 5 minute ablations at 100 W, the lung-tuned antennas showed

similar-sized widths as the liver-tuned antennas (4.4±0.8 vs 4.9±0.5 cm, p=0.34) but had a significantly shorter ablation zone length (5.4±0.5 vs 6.9±0.8 cm, p=0.01). As a result, the lung-tuned antenna created a more spherical ablation zone, although this was not found to be significant (0.80±0.1 vs 0.71±0.14, p=0.38)(Fig. 7).

When comparing the aspect ratio across different time points at 50 W, the study also demonstrated a significant rise in aspect ratio in both the lung-tuned and liver-tuned antenna between 1 minute and 5 minutes (0.43±0.06 vs 0.55±0.06, p=0.007 and 0.37±0.04 vs 0.54±0.09, p=0.001). Within the 100 W group, the change in aspect ratio was found to be larger, where the change in aspect ratio in the lung and liver-tuned antenna between 1 and 5 minutes was also found to be significant (0.55±0.06 vs 0.80±0.1, p=0.002 and 0.55±0.05 vs 0.72±0.5, p=0.03) (Fig. 8).

IV. Discussion and Conclusion

While the majority of existing literature on microwave antenna tuning has been validated in liver tissue, there has been comparatively fewer studies on antenna tuning for lung tissue. This is partially due to the heterogeneous composition of the lung, which contains a mixture of air, blood vessels and lung parenchyma. Further complicating the physiology are the physical deformation of the lung during each respiratory cycle and corresponding changes to the blood and air flow within each lung lobe. In this study, we re-introduced an analytical approach to fabricate a lung-tuned microwave antenna and evaluated its performance at conventional time-power settings that could treat small lesions but minimize the risk for shaft heating and pleural damage. The lung-tuned antenna was validated against a liver-tuned antenna control in an *ex vivo* lung connected to a clinical-grade ventilator, keeping the lung inflated for the entirety of the ablation. The lung-tuned antenna was able to create significantly more spherical ablation zones at 1 min using 50 W, as well as at 5 min at 100 W. This study also showed that despite high reflected power, lung-tuned antennas still offered 15-25% heating efficiency over liver-tuned antennas at the 1 minute time point with both 50 and 100 W, as well as the 5 minute time point with 50 W.

The majority of preclinical lung ablation studies in the past have utilized *ex vivo* deflated lung tissue [21]–[23]. However, a fully deflated lung by itself has similar electrical properties as a liver and can be limited in validating lung-based cancer therapies. The *ex vivo* ventilated lung model presented in this paper is a novel tool that may create a more accurate representation of the lungs compared to strictly deflated lung tissue. By connecting the main bronchus to a ventilator, air can be added into the lung parenchyma in a controlled setting and recapitulate the electrical and thermal properties of the lung. While adding ventilation alone does not account for blood perfusion or lymphatic architecture of the lung, this ventilator controlled *ex vivo* model is a more accurate representation to what is seen in completely-collapsed *ex vivo* models. Success in using a ventilated *ex vivo* model can provide more accurate information on treatment efficacy prior to transitioning *in vivo* models, which can be expensive and resource intensive due to the need for anesthesia and veterinary surveillance.

An *ex vivo* ventilated lung model can provide a similarly controlled and accurate environment at a fraction of the cost and complexity of an *in vivo* porcine lung model.

The amount of reflected power remained higher than expected for the duration of the ablation period. The reason for the mismatch likely lies within the local anatomy of the central aspects of the lung. The lung parenchyma is increasingly heterogeneous centrally, which is made up of proportionally greater volumes of bronchioles, lymphatics and pulmonary vasculature. This is in contrast to the more peripheral regions of the lungs, which are more homogeneous, comprising primarily of air with a small fraction of microvasculature, alveoli and respiratory ducts. As a result, the anatomy in the peripheral lung fields appears homogeneous on even high-resolution CT imaging. Given the small size of the *ex vivo* lungs, the high reflection coefficient most likely resulted from the lung-tuned antennas being placed more centrally and interfacing with a combination of large airways and pulmonary vasculature. Similar trends have been noted in prior clinical studies where higher microwave power and time settings were required to treat lung lesions in the central zone compared to the peripheral zone [17]. In that study, a surrogate metric was used to account for the effects of higher ventilation and perfusion in the central parts of the lungs, where ablation zone sizes appear smaller. The high reflected power recorded in our *ex vivo* lung study fits in line with this clinical trend. Future work in lung-tuning microwave antennas should take into account the higher contribution of blood flow and airways in the central lungs compared to the lung peripheries.

A parametric optimization function was utilized to balance the antenna reflection coefficient with the ablation aspect ratio, metrics that are useful for characterizing antenna performance. While there was a significantly larger aspect ratio using the lung-tuned antenna at the 50 W, 1 minute interval, there was not a significant difference seen between antennas at other power-time combinations. One notable trend was that there was a significant increase in aspect ratio when higher powers or higher time settings were utilized. Utilizing powers of 100 W for 5 minutes led to ablation zones with aspect ratios that averaged 0.8, which was nearly spherical in shape. Future studies that optimize lung ablation shapes should take into account the amount of power that is being delivered to help better modulate the shape over time.

Antenna tuning for microwave ablations in the lung remains an active area of investigation. A prior *in vivo* study of the lungs using an open thoracotomy approach had described a manually-tuned antenna using a triaxial design [13]. An accompanying follow up study also found positive results using lung-tuned triaxial antennas, with the microwave ablation probes were placed near the peripheries of the lungs where the lung parenchyma was more homogeneous [24]. There has been increasing interest in also implementing microwave antenna ablations into flexible antennas for the purpose of bronchoscopically guided ablations [22], [25]. Characterizing temperature-dependent dielectric properties of lung have only begun being investigated, although varying air content within the lung remains unaccounted for [21]. The dielectric properties of a decompressed lung approaches that of the liver, which can be expected given that a decompressed lung has minimal air content. This study utilized a fully expanded lung model to better match the known dielectric and conductivity of a fully inflated lung [26]. However, the fully expanded lung also likely

represents the upper limits of performance for a lung-tuned antenna given that there will be increasing load mismatches that occur during lung decompression. Additional ex vivo validation studies for lung-tuned antenna design will benefit from using ventilator-controlled models, which can control the phase of respiratory cycle during which the ablation is performed.

Many antenna designs have been investigated for the purposes of improving load matching and localized heating to the antenna tip [27]. King et al. developed the first analytical solution and derived the radiation fields of a multi-section insulated antenna in a conductive media. This solution was naturally expanded to interstital monopole and dipole antennas for hyperthermia treatment [28], [29]. Early antenna designs focused on optimized matching to the tissue load and localized heating pattern but its energy delivery efficiency was highly dependent on insertion depth and there was high amounts of backward heating along the antenna shaft from power loss. A well-known alternative to reduce backward heating problem independent of load matching was to electrically connect a metallic choke to the antenna's outer conductor to minimize axial current flow and localize power deposition near the tip of the antenna. The cap choke antenna was described using an annular cap and a coaxial cap in a coaxial antenna – together utilized to match an antenna to a coaxial transmission line [30],[31]. This cap choke design minimized SAR at the insertion point of the catheter antenna and minimized the amount of reflected power up the transmission line. The cap choked antenna design also allowed energy to be delivered into the tissue without being affected by the depth of insertion. A floating sleeve microwave antennas, offered another approach by utilizing a metal conductor that was electrically isolated from the outer connector of the antenna coaxial body, creating a highly localized heating zone independent of insertion depth [32]. The floating sleeve prevented backward heating of the antenna, while creating an efficient ablation zone in the liver. However, many of these designs required a large diameter on the order of 6 or 7 gauge that often precluded its use in percutaneous therapies. Other alternatives to using a choke design to minimize backward heating is to utilize slot antennas. Slot antennas are capable of actively localizing the heating zone to the tip and is also not affected by insertion depth, utilizing overlapping surface currents from each slot [20], [33]. Highly resonant antennas such as the triaxial antenna have also been utilized that can be fabricated with thinner, less invasive designs, and do not require the outer conductor to be connected to the antenna itself [14].

There are notable limitations to this study. For the optimization function, there was a potential risk for singularity in the region of interest. However, we had constrained our function such that the input variables (exposed length) were within the practical limits of fabrication. This was a study performed on a ventilator that kept the air volume constant during the entirety of the ablation. The constant air volume exaggerated the effects of inflation compared to that seen in a physiologic environment where there is constant cycling between inflation and deflation. The results of this study thus likely represent the best-case scenario for a lung-tuned ablation zone given that there was minimal influence of tissue desiccation and no cycling toward lung deflation. Blood flow was also absent in this *ex vivo* lung model. Blood flow normally would act as a strong heat-sink and lead to smaller ablation zones compared to *ex vivo* tissue, which has been well documented in liver tissue. Air within the lungs was accounted for as a function of dielectric, but the cooling effects

from the mass transport of air was not incorporated into the model. These effects can potentially affect the size and shape of the final ablation zone but would require additional investigation into the mass and heat transfer process within the lung. The addition of these other ares of energy transfer should be accounted for in future studies to fully capture the energy transfer from microwave antenna to lung tissue.

V. Conclusions

Locoregional therapy such as microwave ablation for lung malignancies remain an important tool in an interventional oncologist' armament. While advances in lung-tuning for microwave ablations has steadily progressed over the last two decades, there remains substantial room for optimization with regards to the lung parenchyma and anatomy. Antenna designs can be optimized to accommodate for the fraction of air within a specific phase of respiration, as well as localization within a particular lung lobe. in this study, we utilized a novel ventilated *ex vivo* lung model to validate a lung-tuned antenna design. This lung-tuned antenna showed improved heating efficiency compared to a liver-tuned antenna within the ventilated *ex vivo* lung model. Future studies include utilizing the analytic solution to perform real-time adaptive tuning during microwave ablations to improve heating efficiency and ablation shape within the lung. Optimizing lung ablation antenna performance can play a critical role in the final ablation size and margin, directly affecting the risk for local tumor progression in both primary and oligometastatic lung tumors. Continued optimization of lung-tuned microwave antennas will be critical for its continued adoption into clinical practice.

Acknowledgements

This research was supported by NIH UL1TR001881 and the UCLA Radiological Sciences Exploratory Research Program.

Biographies

Jason Chiang received his B.S. in Biomedical Engineering with a focus on electrical engineering at Johns Hopkins University. After receiving a Fulbright Grant to Germany, he obtained his MD, PhD at the University of Wisconsin - Madison. He is currently an interventional radiology resident at UCLA, with an interest in locoregional therapy. His research interests are in using computational modeling to optimize treatments for early-stage solid tumors. He has authored and co-authored many papers in radiology and engineering-based journals and hopes to use engineering principles to help improve patient health. The success of his research has led to multiple NIH, society and industry grant funding.

Lingnan Song is currently the Assistant Professor at Beihang University, P. R. China, in the School of Electronic and Information Engineering. She received the B.S. degree in Optical Engineering from Zhejiang University, P. R. China, in 2014 and the M.S. and Ph.D. degree in Electrical and Computer Engineering from the University of California Los Angeles (UCLA), Los Angeles, CA, USA, in 2016 and 2020 respectively, under the supervision of Prof. Yahya Rahmat-Samii in the Antenna Research, Analysis and Measurement Laboratory. In 2013 she participated in the summer research program at North Carolina State University, where she was involved with the Nanomechanics and Nanoengineering Laboratory and conducted research in developing stretchable and strain-tunable antennas under Prof. Yong Zhu and Prof. Jacob Adams. After joining UCLA, her research focuses on antennas for personal and biomedical applications. Her primary research interests include wireless telemetry antenna systems, implantable antennas, wearable antennas, antenna and human body interactions, RFID, and reconfigurable antennas. Dr. Song has received several awards. She was the recipient of the Distinguished Master's Thesis Award in Physical and Wave Electronics of the year 2016, the First Place winner in the Ernest K. Smith USNC-URSI Student Paper Competition of the year 2017, and the recipient of 2019 International Symposium on Electromagnetic Theory (EMTS) Young Scientist Award.

Feridoun Abtin received his medical degree and completed his radiology residency at Kasturba Medical College. He subsequently received fellowship training in thoracic imaging at UCLA where he stayed on as a faculty member. He is currently a tenured professor in thoracic interventional radiology with an interest in thoracic oncologic intervention. He is known internationally as an expert in minimally invasive treatment of lung cancer, mesothelioma and thymoma. A prolific researcher, he has developed a variety of new and innovative treatments for these diseases and is currently principle investigator on multiple clinical trials in this field. Dr. Abtin is well versed in lung biopsy and thermal ablation of primary and metastatic pulmonary tumors. He utilizes radiofrequency ablation (RFA), microwave ablation (MWA) and cryoablation of thoracic tumors.

Yahya Rahmat-Samii is a Distinguished Professor, a holder of the Northrop-Grumman Chair in electromagnetics, a member of the U.S. National Academy of Engineering (NAE), a Foreign Member of the Chinese Academy of Engineering (CAE) and the Royal Flemish Academy of Belgium for Science and the Arts, the winner of the 2011 IEEE Electromagnetics Field Award, and the Former Chairman of the Electrical Engineering Department, University of California at Los Angeles (UCLA), Los Angeles, CA, USA. He was a Senior Research Scientist with the Caltech/NASA's Jet Propulsion Laboratory. He has authored or coauthored more than 1100 technical journal and conference papers and has written over 36 book chapters and six books and is the holder many patents. He has more than 20 cover-page IEEE publication articles. Dr. Rahmat-Samii received his B.S. degree from University of Tehran and M.S. and Ph.D. degrees from the University of Illinois, Urbana-Champaign, USA.

Prof. Rahmat-Samii is a fellow of IEEE, AMTA, ACES, EMA, and URSI. He was a recipient of the Henry Booker Award from URSI, in 1984, which is given triennially to the most outstanding young radio scientist in North America, the Best Application Paper Prize Award (Wheeler Award) of the IEEE Transactions on Antennas and Propagation in 1992 and 1995, the University of Illinois ECE Distinguished Alumni Award in 1999, the IEEE Third Millennium Medal and the AMTA Distinguished Achievement Award in 2000. In 2001, he received an Honorary Doctorate Causa from the University of Santiago de Compostela, Spain. He received the 2002 Technical Excellence Award from JPL, the 2005 URSI Booker Gold Medal presented at the URSI General Assembly, the 2007 IEEE Chen-To Tai Distinguished Educator Award, the 2009 Distinguished Achievement Award of the IEEE Antennas and Propagation Society, the 2010 UCLA School of Engineering Lockheed Martin Excellence in Teaching Award, and the 2011 campus-wide UCLA Distinguished Teaching Award. He was also a recipient of the Distinguished Engineering Educator Award from The Engineers Council in 2015, the John Kraus Antenna Award of the IEEE Antennas and Propagation Society and the NASA Group Achievement Award in 2016, the ACES Computational Electromagnetics Award and the IEEE Antennas and Propagation S. A. Schelkunoff Best Transactions Prize Paper Award in 2017. Rahmat-Samii was the recipient of the prestigious Ellis Island Medal of Honor in 2019. The medals are awarded annually to a group of distinguished U.S. citizens who exemplify a life dedicated to community service. These are individuals who preserve and celebrate the history, traditions, and values of their ancestry while exemplifying the values of the American way of life and are dedicated to creating a better world. Among the receipts of this honor are seven US presidents to name the few. He is listed in Who's Who in America, Who's Who in Frontiers of Science and Technology and Who's Who in Engineering. He has been a plenary and millennium session speaker at numerous national and international symposia. He has been the organizer and presenter of many successful short courses worldwide. Many of his students have won major theses and conference paper awards.

He has had pioneering research contributions in diverse areas of electromagnetics, antennas, measurements and diagnostics techniques, numerical and asymptotic methods, satellite and personal communications, human/antenna interactions, RFID and implanted antennas in medical applications, frequency-selective surfaces, electromagnetic band-gap and meta-

material structures, applications of the genetic algorithms and particle swarm optimizations. His original antenna designs are on many NASA/JPL space-crafts for planetary, remote sensing, and Cubesat missions. For details visit http://www.antlab.ee.ucla.edu.

He is the designer of the IEEE Antennas and Propagation Society logo which is displayed on all IEEE AP-S publications. He was the 1995 President of the IEEE Antennas and Propagation Society and 2009–2011 President of the United States National Committee (USNC) of the International Union of Radio Science (URSI). He has also served as an IEEE Distinguished Lecturer presenting lectures internationally.

References

[1]. American Cancer Society, “Facts and figures 2020,” Atlanta, Georgia; American Cancer Society, 2020

[2]. Mazzone P, “Preoperative evaluation of the lung resection candidate,” Cleveland Clinic Journal of Medicine, vol. 79 Electronic Suppl 1, pp. eS17–22, May 2012. [PubMed: 22614960]

[3]. Venturini M, Cariati M, Marra P, Masala S, Pereira PL, and Car-rafiello G, “Cirse standards of practice on thermal ablation of primary and secondary lung tumours,” CardioVascular and Interventional Radiology, pp. 1–17, 2020.

[4]. Ahmed M, “Image-guided tumor ablation: standardization of terminology and reporting criteria—a 10-year update: supplement to the consensus document,” Journal of Vascular and Interventional Radiology, vol. 11, no. 25, pp. 1706–1708, 2014.

[5]. Dupuy DE, Fernando HC, Hillman S, Ng T, Tan AD, Sharma A, Rilling WS, Hong K, and Putnam JB, “Radiofrequency ablation of stage ia non-small cell lung cancer in medically inoperable patients: Results from the american college of surgeons oncology group z4033 (alliance) trial,” Cancer, vol. 121, no. 19, p. 3491–3498, Oct 2015. [PubMed: 26096694]

[6]. Brace CL, “Radiofrequency and microwave ablation of the liver, lung, kidney, and bone: what are the differences?” Curr Probl Diagn Radiol, vol. 38, no. 3, p. 135–43, 2009. [PubMed: 19298912]

[7]. Brace CL, Diaz TA, Hinshaw JL, and Lee FT, “Tissue contraction caused by radiofrequency and microwave ablation: a laboratory study in liver and lung,” Journal of Vascular and Interventional Radiology: JVIR, vol. 21, no. 8, p. 1280–1286, Aug 2010. [PubMed: 20537559]

[8]. Macchi M, Belfiore MP, Floridi C, Serra N, Belfiore G, Carmignani L, Grasso RF, Mazza E, Pusceddu C, Brunese L, and et al. , “Radiofrequency versus microwave ablation for treatment of the lung tumours: Lumira (lung microwave radiofrequency) randomized trial,” Medical Oncology (Northwood, London, England), vol. 34, no. 5, p. 96, May 2017.

[9]. Wolf FJ, Grand DJ, Machan JT, Dipetrillo TA, Mayo-Smith WW, and Dupuy DE, “Microwave ablation of lung malignancies: effectiveness, ct findings, and safety in 50 patients,” Radiology, vol. 247, no. 3, p. 871–879, Jun 2008. [PubMed: 18372457]

[10]. Lu Q, Cao W, Huang L, Wan Y, Liu T, Cheng Q, Han Y, and Li X, “Ct-guided percutaneous microwave ablation of pulmonary malignancies: Results in 69 cases,” World Journal of Surgical Oncology, vol. 10, p. 80, May 2012. [PubMed: 22564777]

[11]. Nevels RD, Arndt GD, Raffoul GW, Carl JR, and Pacifico A, “Microwave catheter design,” IEEE Transactions on Biomedical Engineering, vol. 45, no. 7, pp. 885–890, 1998. [PubMed: 9644897]

[12]. Labonte S, Blais A, Legault SR, Ali HO, and Roy L, “Monopole antennas for microwave catheter ablation,” IEEE transactions on microwave theory and techniques, vol. 44, no. 10, pp. 1832–1840, 1996.

[13]. Durick NA, Laeseke PF, Broderick LS, Lee FT Jr, Sampson LA, Frey TM, Warner TF, Fine JP, Van der Weide DW, and Brace CL, “Microwave ablation with triaxial antennas tuned for lung: results in an in vivo porcine model,” Radiology, vol. 247, no. 1, pp. 80–87, 2008. [PubMed: 18292471]

[14]. Brace CL, van der Weide DW, Lee FT, Laeseke PF, and Sampson L, “Analysis and experimental validation of a triaxial antenna for microwave tumor ablation,” in 2004 IEEE

MTT-S International Microwave Symposium Digest (IEEE Cat. No. 04CH37535), vol. 3. IEEE, 2004, pp. 1437–1440.

[15]. Etoz S and Brace CL, "Analysis of microwave ablation antenna optimization techniques," International Journal of RF and Microwave Computer-Aided Engineering, vol. 28, no. 3, p. e21224, 2018.

[16]. Bertram JM, Yang D, Converse MC, Webster JG, and Mahvi DM, "A review of coaxial-based interstitial antennas for hepatic microwave ablation," Crit Rev Biomed Eng, vol. 34, no. 3, p. 187–213, 2006. [PubMed: 16930124]

[17]. Al-Hakim RA, Abtin FG, Genshaft SJ, Kutay E, and Suh RD, "Defining new metrics in microwave ablation of pulmonary tumors: Ablation work and ablation resistance score," vol. 27, no. 9, pp. 1380–1386.

[18]. King RW, Trembly B, and Strohbehn J, "The electromagnetic field of an insulated antenna in a conducting or dielectric medium," IEEE Transactions on Microwave Theory and Techniques, vol. 31, no. 7, pp. 574–583, 1983.

[19]. King RW, "Theory of the terminated insulated antenna in a conducting medium," IEEE Transactions on Antennas and Propagation, vol. 12, no. 3, pp. 305–318, 1964.

[20]. Brace CL, "Dual-slot antennas for microwave tissue heating: parametric design analysis and experimental validation," Medical Physics, vol. 38, no. 7, p. 4232–4240, Jul 2011. [PubMed: 21859025]

[21]. Sebek J, Bortel R, and Prakash P, "Broadband lung dielectric properties over the ablative temperature range: Experimental measurements and parametric models," Medical physics, vol. 46, no. 10, pp. 4291–4303, 2019. [PubMed: 31286530]

[22]. Yuan H-B, Wang X-Y, Sun J-Y, Xie F-F, Zheng X-X, Tao G-Y, Pan L, and Hogarth DK, "Flexible bronchoscopy-guided microwave ablation in peripheral porcine lung: a new minimally-invasive ablation," Translational Lung Cancer Research, vol. 8, no. 6, p. 787–796, Dec 2019. [PubMed: 32010557]

[23]. Gao X, Tian Z, Cheng Y, Geng B, Chen S, and Nan Q, "Experimental and numerical study of microwave ablation on ex-vivo porcine lung," Electromagnetic Biology and Medicine, vol. 38, no. 4, p. 249–261, 2019. [PubMed: 31554439]

[24]. Brace CL, "Radiofrequency and microwave ablation of the liver, lung, kidney, and bone: what are the differences?" Current problems in diagnostic radiology, vol. 38, no. 3, pp. 135–143, 2009. [PubMed: 19298912]

[25]. Ferguson J, Egressy K, Schefelker R, Thiel M, Thom M, Bissing J, Brace C, and Lee F, "Bronchoscopically-guided microwave ablation in the lung," CHEST, vol. 144, no. 4, p. 87a, Oct 2013. [PubMed: 23392731]

[26]. Gabriel S, Lau RW, and Gabriel C, "The dielectric properties of biological tissues: Ii. measurements in the frequency range 10 hz to 20 ghz," Physics in Medicine and Biology, vol. 41, no. 11, p. 2251–2269, Nov 1996. [PubMed: 8938025]

[27]. Bertram JM, Yang D, Converse MC, Webster JG, and Mahvi DM, "A review of coaxial-based interstitial antennas for hepatic microwave ablation," Critical Reviews™ in Biomedical Engineering, vol. 34, no. 3, 2006.

[28]. Iskander MF and Tumeh AM, "Design optimization of interstitial antennas," IEEE Trans Biomed Eng, vol. 36, no. 2, p. 238–46, Feb 1989. [PubMed: 2917769]

[29]. Cherry PC and Iskander MF, "Calculations of heating patterns of an array of microwave interstitial antennas," IEEE Trans Biomed Eng, vol. 40, no. 8, p. 771–9, 1993. [PubMed: 8258443]

[30]. Pisa S, Cavagnaro M, Bernardi P, and Lin JC, "A 915-mhz antenna for microwave thermal ablation treatment: physical design, computer modeling and experimental measurement," IEEE Trans Biomed Eng, vol. 48, no. 5, p. 599–601, May 2001. [PubMed: 11341534]

[31]. Lin JC and Wang YJ, "The cap-choke catheter antenna for microwave ablation treatment," IEEE transactions on bio-medical engineering, vol. 43, no. 6, p. 657–660, Jun 1996. [PubMed: 8987271]

[32]. Yang D, Bertram JM, Converse MC, O'Rourke AP, Webster JG, Hagness SC, Will JA, and Mahvi DM, "A floating sleeve antenna yields localized hepatic microwave ablation," IEEE Trans Biomed Eng, vol. 53, no. 3, p. 533–7, Mar 2006. [PubMed: 16532780]

[33]. Saito K, Hayashi Y, Yoshimura H, and Ito K, "Heating characteristics of array applicator composed of two coaxial-slot antennas for microwave coagulation therapy," IEEE Trans. Microw. Theory Tech, vol. 48, p. 1800–1806, 2000.

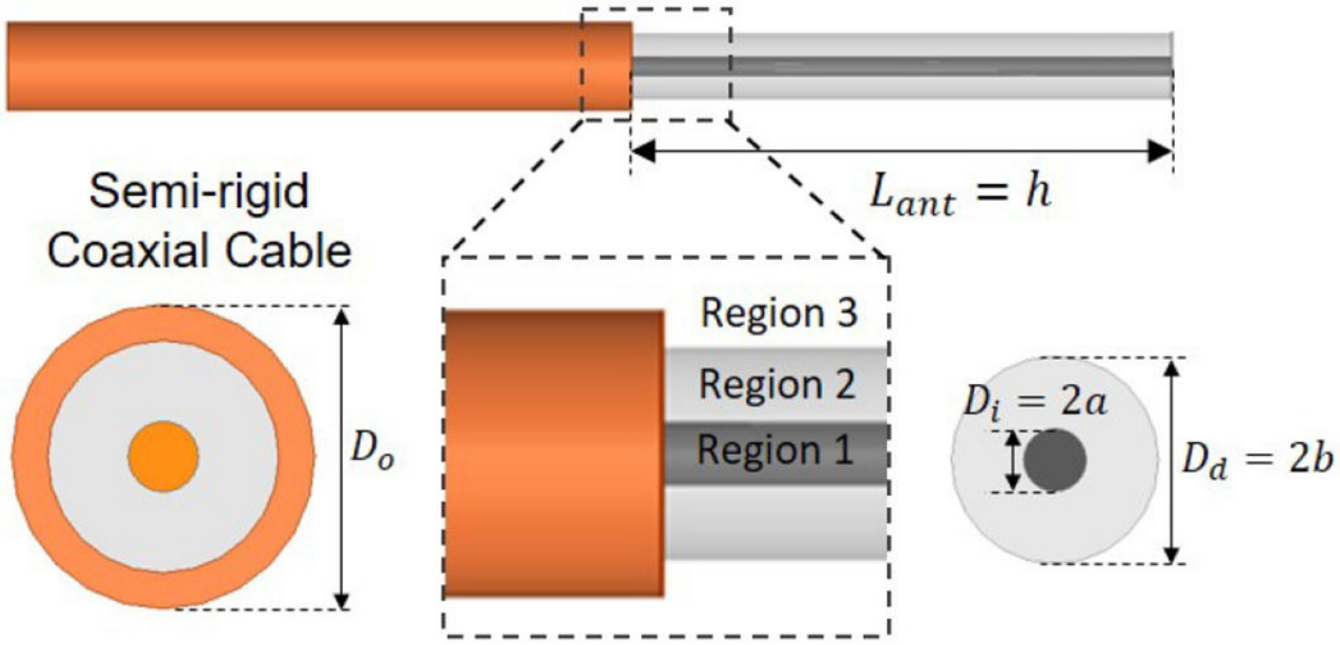

Fig. 1.

Coaxial monopole antenna formed by stripping off a section of outer conductor at the end of coaxial cable by $\lambda_{eff}/4$, with the dimensions corresponding to 0.085" standard listed in Table I. Region 1, 2 and 3 correspond to the inner conductor, PTFE dielectric material and lossy organ tissue (lung or liver), respectively.

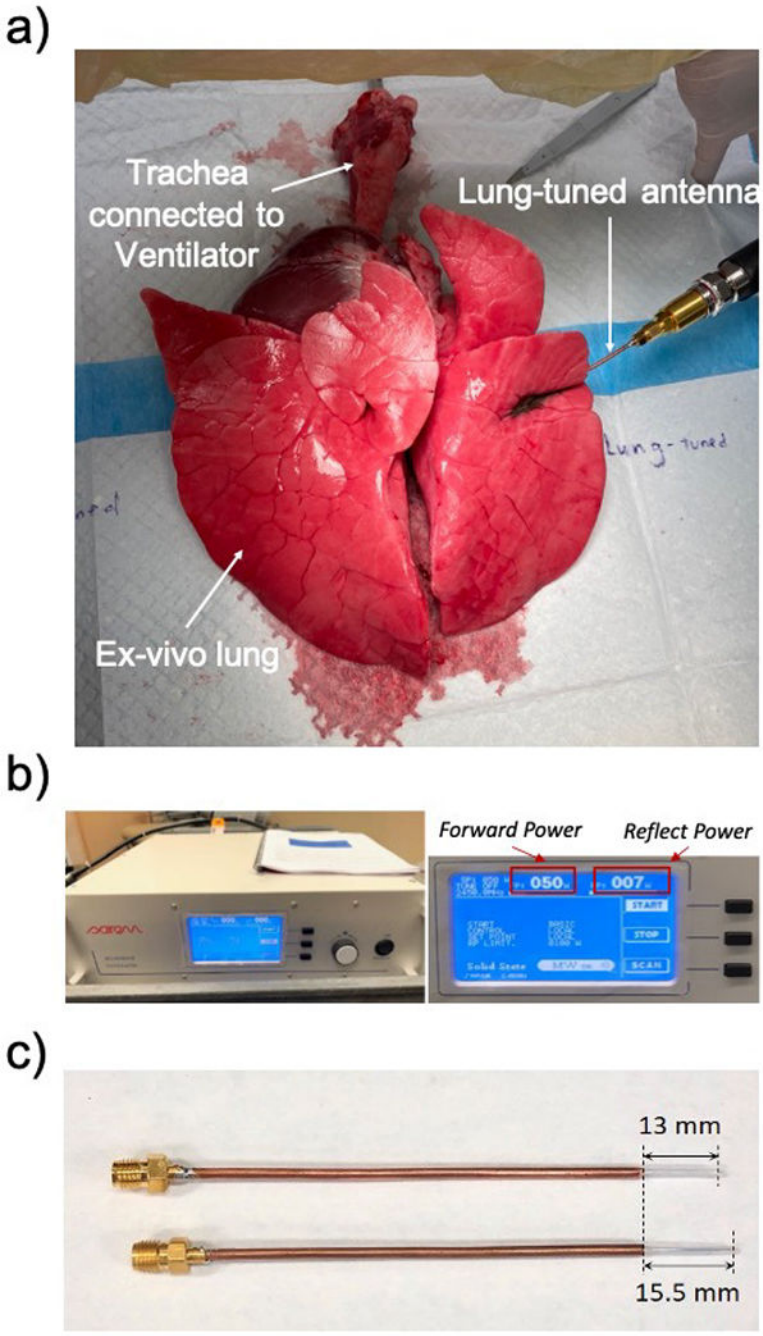

Fig. 2.

a) Sample set up of the *ex vivo* porcine lung study and positioning of the microwave antenna within the lung parenchyma. b) The microwave generator with real-time forward and backward power displayed. c) Images of the liver-tuned and lung-tuned monopole antennas, with exposed monopole lengths of 13 mm and 15.5 mm, respectively.

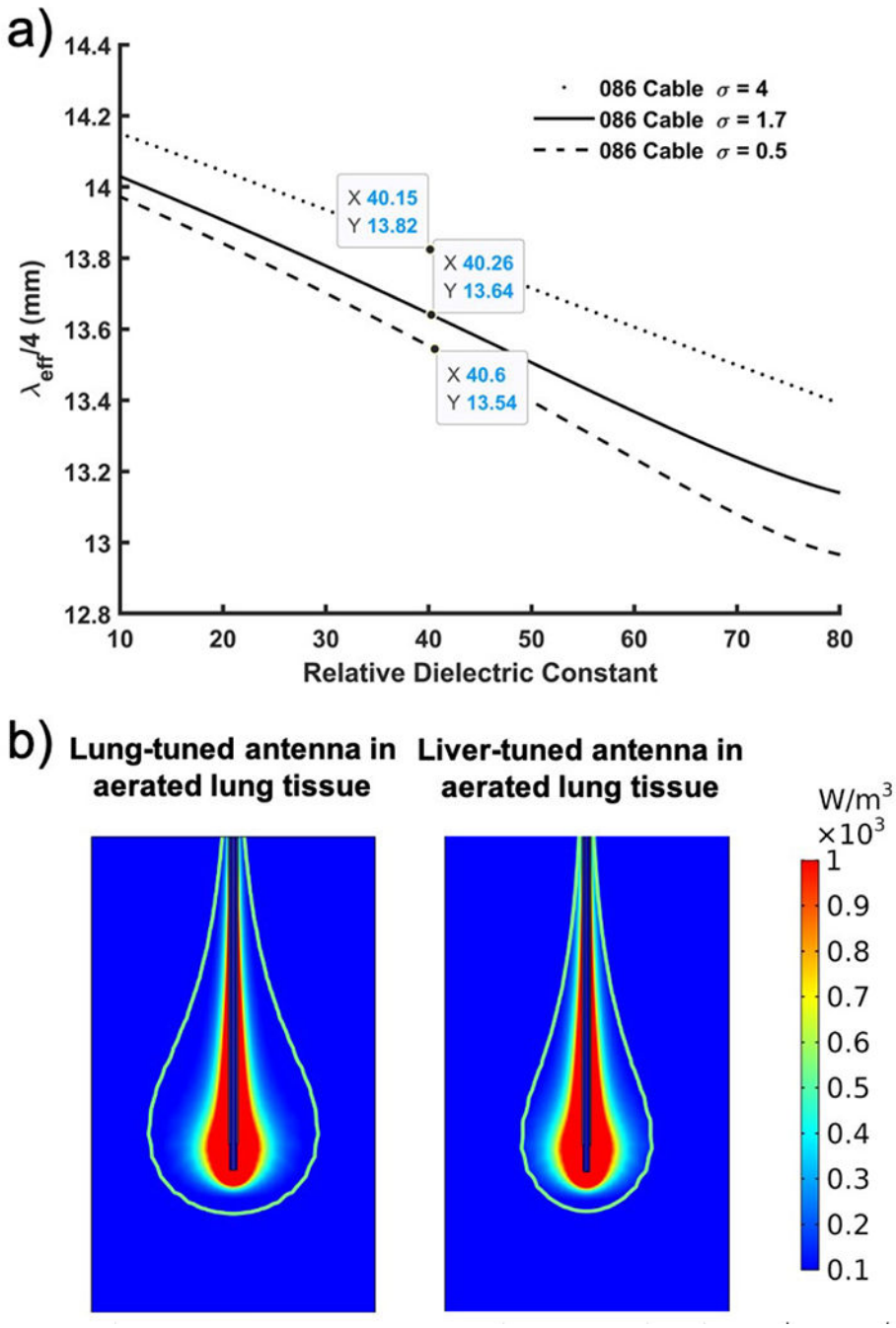

Fig. 3.

a) The effective quarter wavelength computed with $\lambda_{eff}/4 = \pi/2\beta_{eff}$, for the coaxial antenna consisting of an inner conductor wrapped with dielectric coating and inserted into lossy dielectric medium. Note that the exposed length of the dielectric was insensitive to large variations in conductivity and relative dielectric constant. b) Specific absorption rate (SAR) mapping of a microwave ablation zone in an air-filled lung parenchyma using a lung-tuned antenna (left) and a liver-tuned antenna (right). The green isocontour line represents the 300 W/kg SAR used to calculate the aspect ratio. The maximum diameter of the lung-tuned

antenna based on the isocontour was 1.2 cm, compared to 0.70 cm in the liver-tuned antenna.

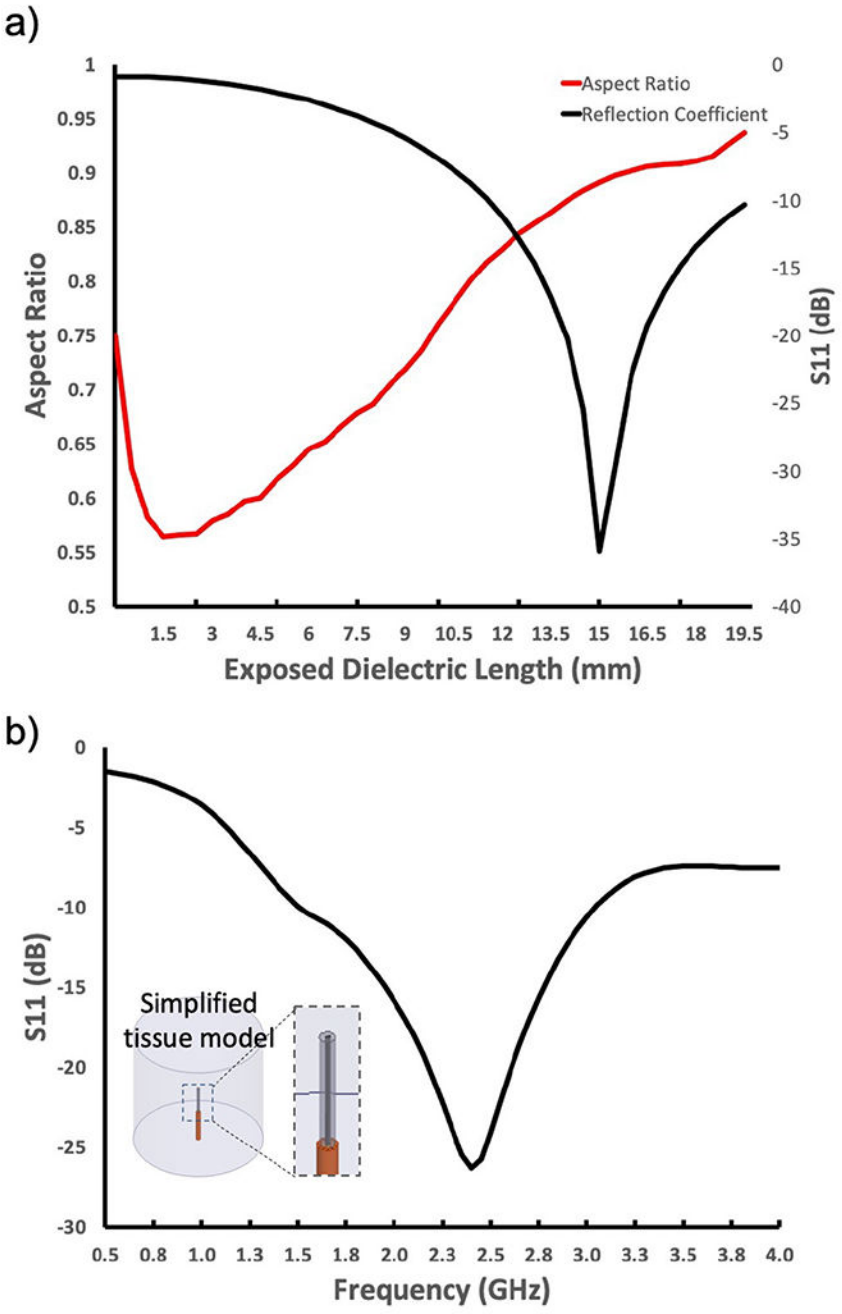

Fig. 4.

a) Chart showing the reflection coefficient (S11) and aspect ratio as a function of increasing exposed dielectric length. b) Reflection coefficient (dB) as a function of operating frequency. An example of the tissue model used to calculate the reflection coefficient is also shown. The cost function was utilized to weigh the benefit of each performance metric to provide the best organ-tuned antenna performance.

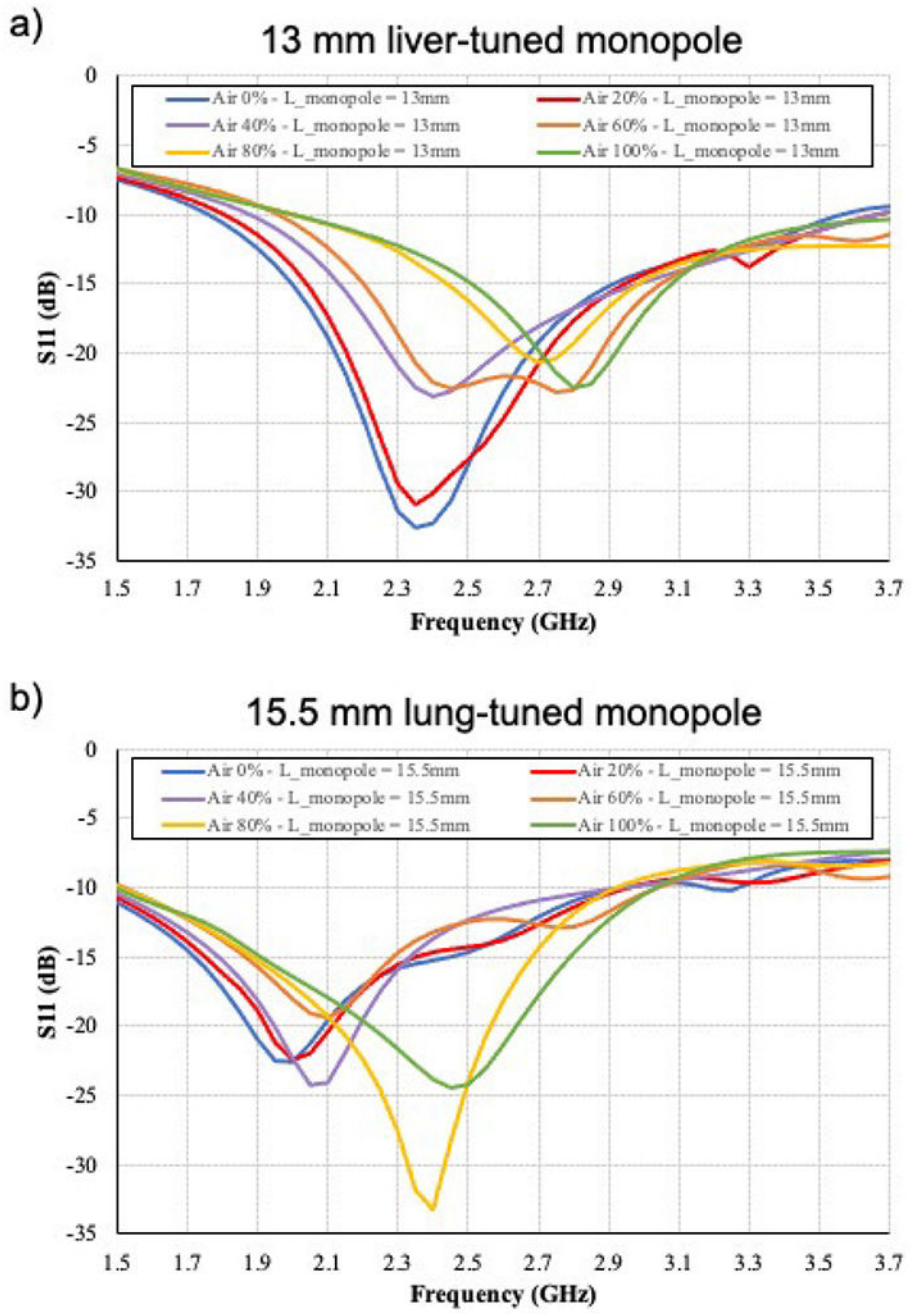

Fig. 5.

Simulations of the S parameter vs frequency for the 6 air content states utilizing the 13 mm and 15.5 mm monopole lengths. The 15.5 mm monopole resulted in an optimal S11 for high air content (80% and 100% air filling), while the 13 mm monopole antenna had an optimal S11 in a deflated lung.

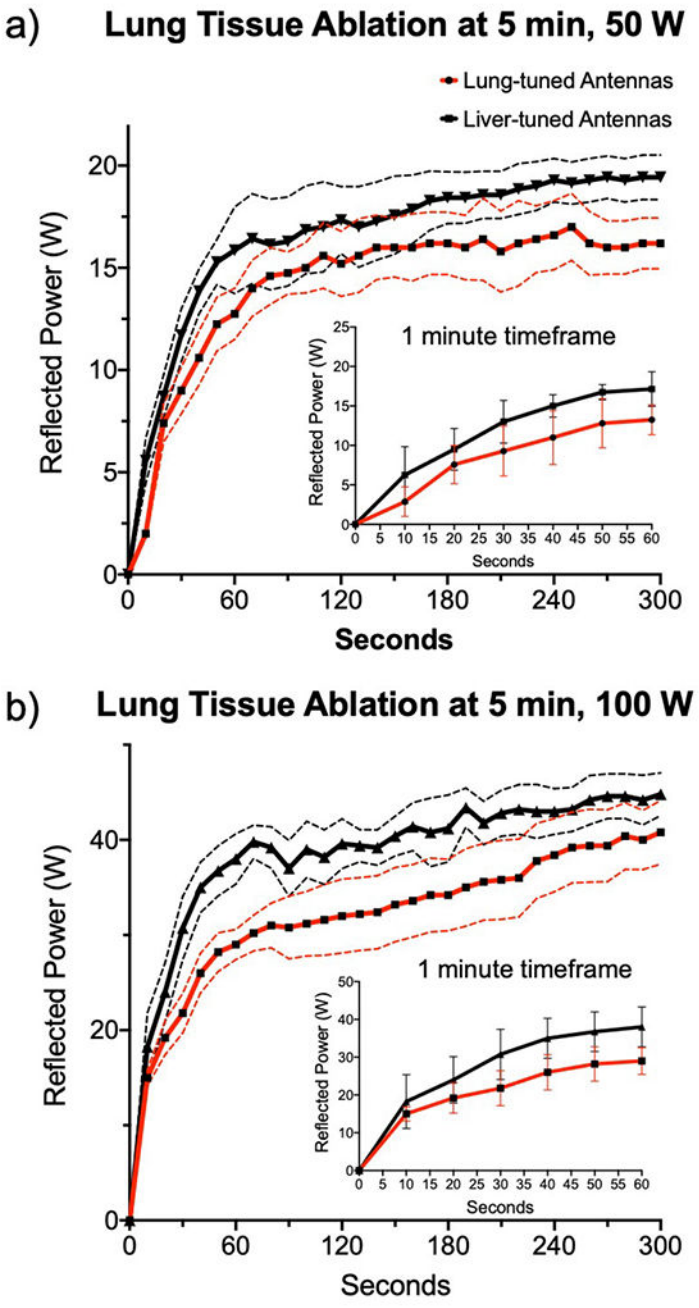

Fig. 6.

Reflected power at 2.45 GHz across each organ-tuned antenna using the *ex vivo* ventilated porcine lung model at: (a) 50 W for 5 minutes (top) with a magnified view of the first minute (inset image) and (b) 100 W for 5 minutes with the corresponding magnified view of the first minute (inset image). The dashed lines specify the upper and lower bounds of the reflected power. In general, the lung-tuned antenna was found to be more efficient in delivering microwave energy, recording less reflected power compared to the liver-tuned antenna. In the 50 W group, this difference in reflected power was found to be significant

at both the 1 minute and 5 minutes while in the 100 W group, there was significantly less power reflected only at the 1 minute time point.

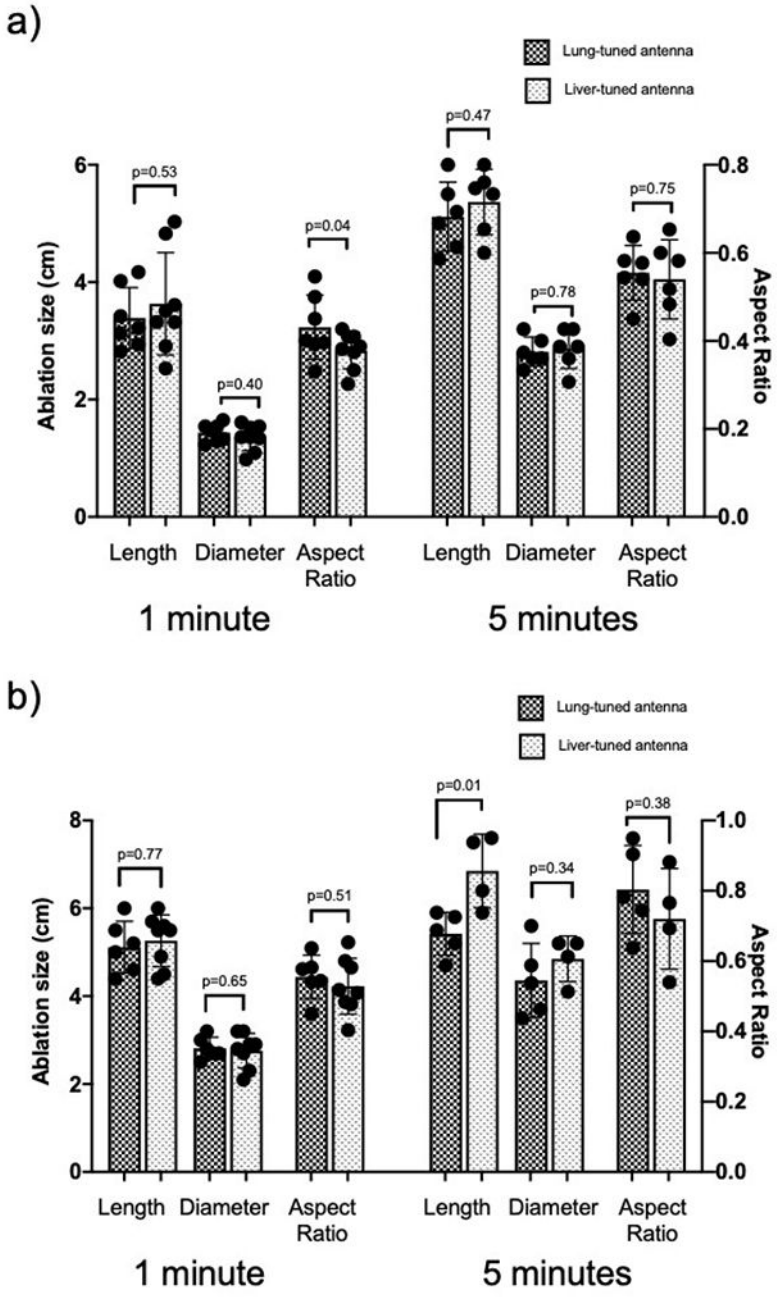

Fig. 7.

Microwave ablation size in lung tissue over a period of 1 and 5 minutes using: (a) 50 W and (b) 100 W. The lung-tuned antenna created significantly more spherical ablation zones compared to the liver-tuned antenna at the 1 minute time point using 50 W. There was a significant rise in ablation zone sphericity in both antenna types as power and time was increased. P-values less than 0.05 were deemed significant.

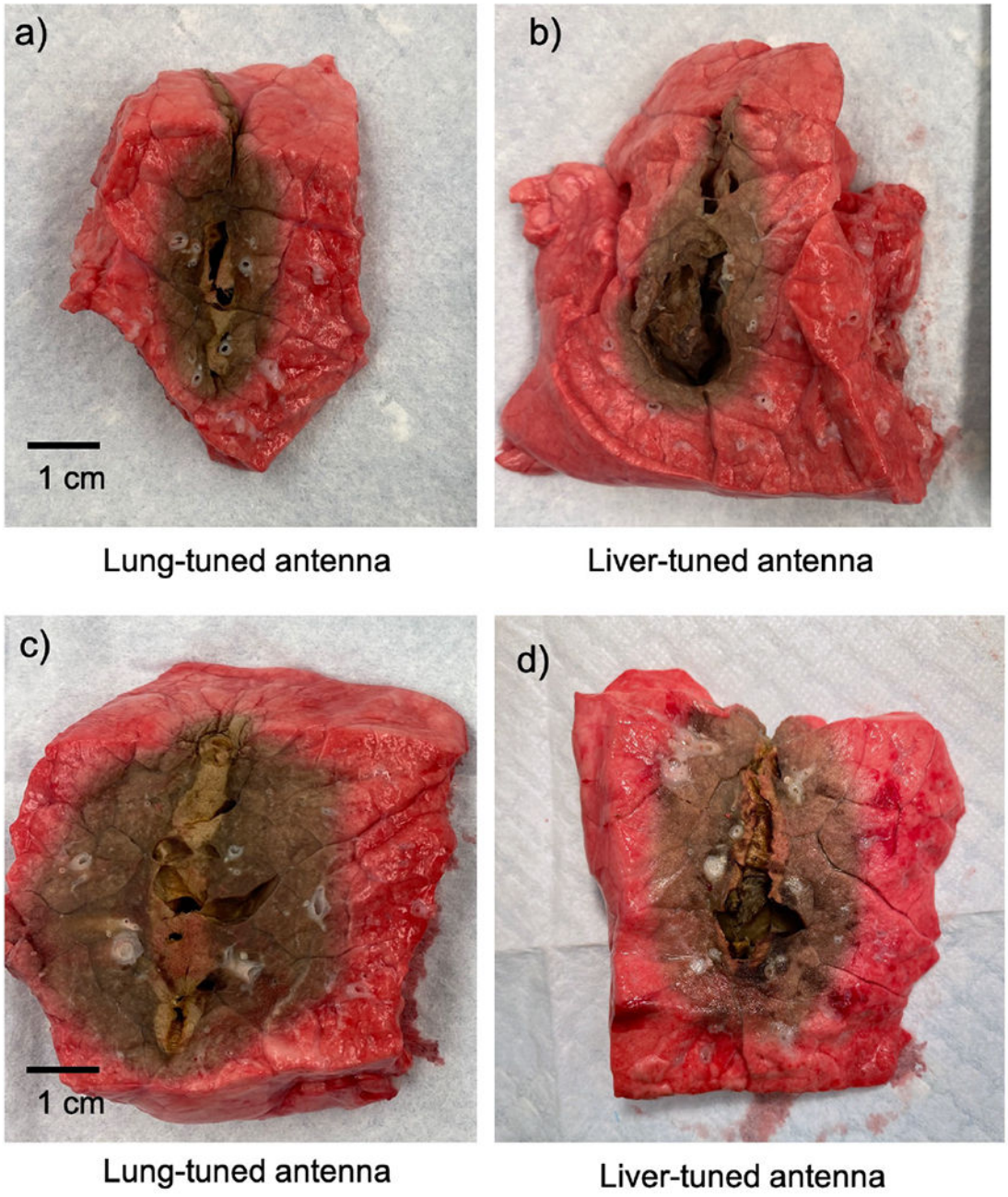

Fig. 8.

Samples of ablated lung tissue at the following ablation parameters: a) Lung-tuned antenna at 100 W for 1 minute, b) Liver-tuned antenna at 100 W for 1 minute, c) Lung-tuned antenna at 100 W for 5 minutes and d) Liver-tuned antenna at 100 W for 5 minutes. While there was not a significant difference in ablation dimension or aspect ratio between the two antennas using 100 W at the 1 minute time point, the lung-tuned antennas created a significantly more spherical ablation zone compared to the liver-tuned antennas at 5 minutes. This may

be related to improved energy delivery seen in the lung-tuned antenna compared to the liver-tuned antenna.

TABLE I

THE DIMENSIONS OF COAXIAL CABLE WITH THE 086 STANDARDS AND THE DIELECTRIC PROPERTIES FOR LUNG AND LIVER TISSUES.

Cable	Dielectric ϵ_r	D_i (mm)	D_d (mm)	D_o (mm)
0.085”	2.1	0.51	1.68	2.21

Tissue	Relative Permittivity	Conductivity (S/m)	Notes
Liver	48	1.7	Normal
Lung	20.5	0.804	Inflated
	48.4	1.680	Deflated